CHEMISTRY

Interstellar formation of glyceric acid [$HOCH_2CH(OH)COOH$]—The simplest sugar acid

Jia Wang[1,2], Joshua H. Marks[1,2], Ryan C. Fortenberry[3]*, Ralf I. Kaiser[1,2]*

Glyceric acid [$HOCH_2CH(OH)COOH$]—the simplest sugar acid—represents a key molecule in biochemical processes vital for metabolism in living organisms such as glycolysis. Although critically linked to the origins of life and identified in carbonaceous meteorites with abundances comparable to amino acids, the underlying mechanisms of its formation have remained elusive. Here, we report the very first abiotic synthesis of racemic glyceric acid via the barrierless radical-radical reaction of the hydroxycarbonyl radical ($HO\dot{C}O$) with 1,2-dihydroxyethyl ($HO\dot{C}HCH_2OH$) radical in low-temperature carbon dioxide (CO_2) and ethylene glycol ($HOCH_2CH_2OH$) ices. Using isomer-selective vacuum ultraviolet photoionization reflectron time-of-flight mass spectrometry, glyceric acid was identified in the gas phase based on the adiabatic ionization energies and isotopic substitution studies. This work reveals the key reaction pathways for glyceric acid synthesis through nonequilibrium reactions from ubiquitous precursor molecules, advancing our fundamental knowledge of the formation pathways of key biorelevant organics—sugar acids—in deep space.

INTRODUCTION

Since the first identification of the simplest sugar acid—glyceric acid [$HOCH_2CH(OH)COOH$, **1**]—in the Murchison and Murray meteorites by Cooper *et al.* (*1*) more than 20 years ago, **1** has been at the center of attention from the astronomy, astrobiology, and laboratory astrochemistry communities (*2*–*7*). **1** plays a key role in contemporary biochemical processes vital to cellular metabolism such as glycolysis (Fig. 1). It serves as the starting point to synthesis of 2-phosphoglyceric acid ($C_3H_7O_7P$, **2**) and 3-phosphoglyceric acid ($C_3H_7O_7P$, **3**) via phosphorylation (*8*). **1** plays a central role in glycolysis, the tricarboxylic acid (TCA) cycle, and photosynthesis in the Calvin cycle, contributing to carbon metabolism (TCA cycle), carbon fixation, and sugar phosphate production (*9*). Through nucleophilic substitution, **1** may react with ammonia (NH_3) to yield the proteinogenic amino acid serine [$HOCH_2CH(NH_2)COOH$, **4**], eventually producing complex amino acids and peptides. Through the oxidation with nicotinamide adenine dinucleotide (NAD^+), **1** can be formed from glyceraldehyde [$HOCH_2CH(OH)CHO$, **5**], which can then be reduced by nicotinamide adenine dinucleotide phosphate ($NADP^+$) to glycerol [$HOCH_2CH(OH)CH_2OH$, **6**]—a key molecular precursor to phospholipids—the main component of cell membranes (*10*, *11*).

In prebiotic chemistry, **1** may have served as a fundamental building block for crucial biomolecules (Fig. 1) (*8*). The methylation of **1** can form deoxy sugar acids such as 2-methyl glyceric acid [$HOCH_2C(CH_3)(OH)COOH$), **7**]. Undergoing carbon-carbon bond cleavage, **1** can be converted into formic acid ($HCOOH$, **8**) and glycolic acid ($HOCH_2COOH$, **9**). Recently, Marks *et al.* (*12*) revealed the formation of **9** in irradiated interstellar model ices of carbon dioxide (CO_2) and methanol (CH_3OH, **10**); **9** was formed through barrierless radical-radical recombination of the hydroxycarbonyl radical ($HO\dot{C}O$, **11**) with the hydroxymethyl ($\dot{C}H_2OH$) radical. Oxidation of **1** results in the formation of biorelevant hydroxypyruvic acid [$HOCH_2C(O)COOH$, **12**] and tartronic acid [$HOOCCH(OH)COOH$, **13**] (*13*), which can be decarboxylated into **9**. Further, the cleavage of the carbon-oxygen bond in **1** prepares 3-hydroxypropionic acid ($HOCH_2CH_2COOH$, **14**) and the biomolecule lactic acid [$CH_3CH(OH)COOH$, **15**] (*14*).

Glyceric acid (**1**) is a simple representative of sugar-related compounds and can form from the simplest sugar molecule glyceraldehyde (**5**) via oxidation (Fig. 1). Sugar acids and sugar alcohols are vital precursors to the molecular building blocks of biomolecules and could have seeded the evolution of life as we know it (*15*). Therefore, the elucidation of their formation routes can aid in understanding the molecular mass growth processes of astrobiologically relevant molecules necessary for the origins of life. Among some 300 molecules identified in the interstellar medium (ISM) (*16*), sugar-related molecules such as glycolaldehyde ($HCOCH_2OH$) have been identified toward the molecular core Sagittarius B2 (*17*, *18*). Although **1** has not yet been identified in the ISM (*16*), it has been observed in laboratory simulation experiments. Ices composed of electron-irradiated methanol (**10**) ice (*4*) and ultraviolet-irradiated ice mixtures of **10**, ammonia (NH_3), and water (H_2O) (*19*, *20*) reveal its formation through the hydrolysis of organic residues remaining after temperature-programmed desorption (TPD) to room temperature. Furthermore, **1** has been identified in the hydrolyzed organic matter of carbonaceous chondrites with an abundance (80 nmol g^{-1}) comparable to amino acids (*1*), indicating that **1** is able to survive the entrance of the meteorite into the atmosphere of the early Earth when embedded in a matrix (*21*). However, unraveling the abiotic formation mechanisms of molecular **1** in interstellar analog ices is still elusive. Under interstellar conditions, the formation of biologically relevant molecules is feasible via abiotic (nonbiological) reaction mechanisms, in which these molecules can be formed in interstellar ices composed of simple organic molecules when subjected to ionizing radiation. This understanding is of fundamental importance to the astronomy and astrochemistry communities to rationalize the origin and formation routes of biorelevant molecules linked to the origins of life and the simplest sugar acid **1** in particular.

Here, we demonstrate the very first abiotic synthesis of **1** in low-temperature (5 K) carbon dioxide and ethylene glycol ($HOCH_2CH_2OH$, **16**) ice mixtures. This was accomplished via the barrierless radical-radical

[1]W. M. Keck Research Laboratory in Astrochemistry, University of Hawaii at Manoa, Honolulu, HI 96822, USA. [2]Department of Chemistry, University of Hawaii at Manoa, Honolulu, HI 96822, USA. [3]Department of Chemistry and Biochemistry, University of Mississippi, University, MS 38677, USA.
*Corresponding author. Email: r410@olemiss.edu (R.C.F.); ralfk@hawaii.edu (R.I.K.)

reaction of the hydroxycarbonyl (HOĊO, **11**) with the 1,2-dihydroxyethyl (HOĊHCH$_2$OH, **17**) radicals (Figs. 1 and 2). These model ices were exposed to energetic electrons mimicking secondary electrons generated in the track of galactic cosmic rays (GCRs) penetrating ices in cold molecular clouds aged a few million years (*22*). By merging our experiments with calculations, **1** was identified in the gas phase through vacuum ultraviolet (VUV) photoionization reflectron time-of-flight mass spectrometry (PI-ReTOF-MS) during the TPD of irradiated ices based on computed adiabatic ionization energies (IEs) and isotopic substitution studies. This finding notably advances the knowledge of the formation pathways of key biorelevant organics—sugar acids—in deep space. Carbon dioxide is one of the most ubiquitous molecules in interstellar ices and has been detected at fractions of up to 40% with respect to water toward the AFGL 989 source (*23*). Ethylene glycol (**16**) generated via radical-radical recombination of the hydroxymethyl (ĊH$_2$OH) radicals (*4*, *24*) is abundant in the ISM, Murchison meteorites, and comets (*1*, *18*, *25*); the abundance of **16** has been found to be 0.25% with respect to water in the Comet C/1995 O1 (Hale-Bopp) (*26*). Therefore, the formation of **1** in interstellar ices containing carbon dioxide and ethylene glycol represents a plausible mechanistic pathway as demonstrated here. Once formed, **1** can be incorporated into planetesimals and ultimately delivered to planets like early Earth via meteorites, thus participating in a complex chain of chemical reactions leading to the molecular precursors important for the origins of life.

RESULTS

Infrared spectroscopy

Fourier transform infrared (FTIR) spectroscopy was used to monitor the chemical evolution of the ices before (black line) and after (red line) the irradiation (figs. S1 to S4). Detailed assignments of the FTIR

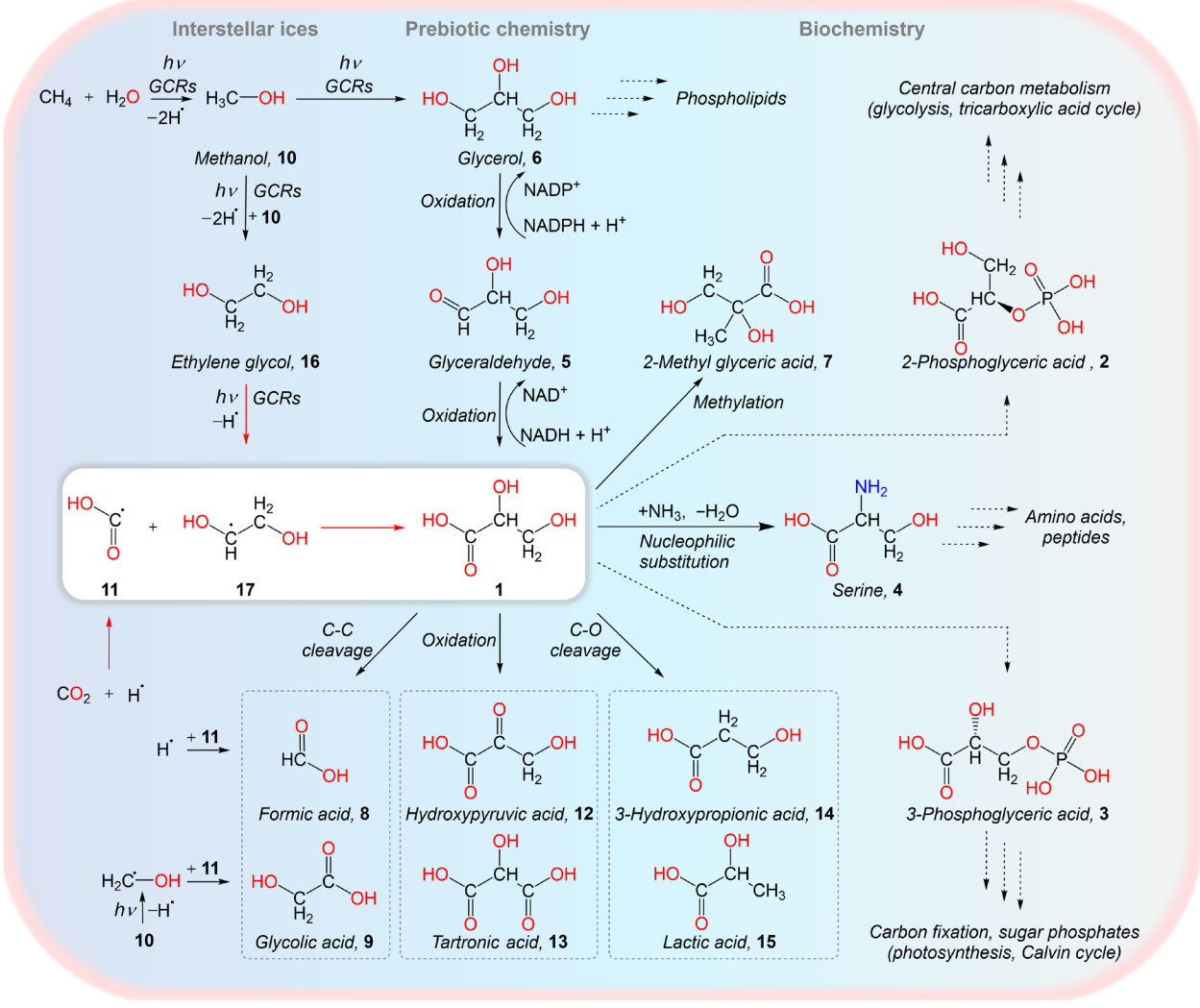

Fig. 1. Formation of glyceric acid in interstellar ices. The preparation of glyceric acid (**1**) in low-temperature ices containing carbon dioxide and ethylene glycol (**16**) is accomplished through energetic processing by GCR proxies. This process involves carbon-carbon bond coupling via recombination of the hydroxycarbonyl radical (HOĊO, **11**) with the 1,2-dihydroxyethyl radical (HOĊHCH$_2$OH, **17**). Glyceric acid (**1**) serves as a precursor for critical biomolecules including the proteinogenic amino acid serine (**4**), 2-methyl glyceric acid (**7**), and lactic acid (**15**). In contemporary biochemistry, glyceric acid further represents molecular building blocks of 2-phosphoglyceric acid (**2**) and 3-phosphoglyceric acid (**3**) via phosphorylation reactions, linking to the TCA cycle (top right) and Calvin cycle (bottom right), respectively.

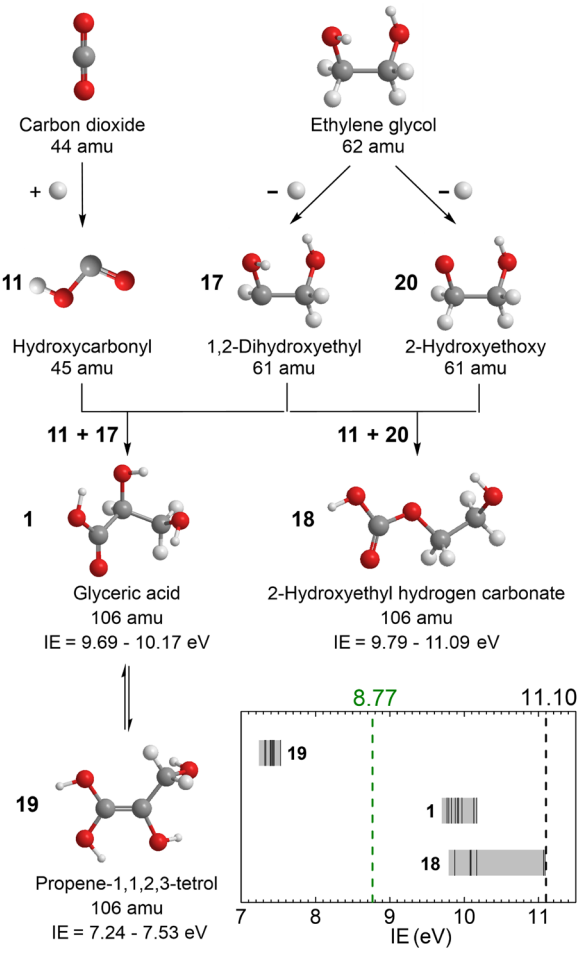

Fig. 2. Reaction scheme leading to three $C_3H_6O_4$ (m/z = 106) isomers (1, 18, 19) in irradiated carbon dioxide–ethylene glycol ices. Barrierless radical-radical reactions **11** plus **17** and **11** plus **20** produce **1** and **18**, respectively; tautomerization of **1** may lead to the enol **19**. The adiabatic IEs are computed at the CCSD(T)-F12b/cc-pVTZ-F12//B3LYP/aug-cc-pVTZ level of theory including zero-point vibrational energies and are corrected by incorporating error (table S4). The insert (bottom right) compiles the computed IEs of isomers (black solid line) and ranges of the conformers (gray area) after error analysis. VUV photon energies (dashed lines) at 11.10 and 8.77 eV were used to photoionize subliming molecules during the TPD process.

spectra are summarized in tables S1 to S4. The absorptions of the deposited ices can be attributed to the fundamentals and combination modes of carbon dioxide and ethylene glycol (**16**). After irradiation at 5 K, several absorption features were detected. The region between 2200 and 1400 cm^{-1} can be deconvoluted into several Gaussian peaks (fig. S1B). The infrared absorption band at 2140 cm^{-1} is assigned to the stretch of carbon monoxide (CO); this is confirmed from the observation of $C^{18}O$ at 2090 cm^{-1} and ^{13}CO at 2092 cm^{-1} (figs. S2B and S4B) (*27*). The absorptions at 1767 and 1657 cm^{-1} are linked to the formation of one or more carbonyl (C═O)–containing species and the bending mode (ν_2) of water, respectively (*12*). After accounting for vibrational anharmonicity at the B3LYP/aug-cc-pVTZ level of theory, the strongest vibration mode of **1** is predicted at 1803 cm^{-1} for **1g**, i.e., the lowest energy conformer of **1** (table S5). Since vibrational frequencies of matrix-isolated species are often shifted from their gas-phase values (*28*) and FTIR absorptions can be broadened because of the ice matrix, the anharmonic frequency is close to the observed absorptions at 1767 cm^{-1}, indicating that this absorption may be linked to **1** in a polar environment. The absorptions at 1722 and 1500 cm^{-1} are associated with the CO stretching mode (ν_2) and CH_2 bending mode (ν_3) of formaldehyde (H_2CO) (*27*, *29*); these features can also be identified in deuterium-labeled (fig. S3) and ^{13}C-labeled (fig. S4) ices through absorptions at 1703 cm^{-1} (D_2CO, ν_2), 1681 cm^{-1} ($H_2{}^{13}CO$, ν_2), and 1500 cm^{-1} ($H_2{}^{13}CO$, ν_3) (*12*, *27*, *29*, *30*). The absorptions at 1849 cm^{-1} in processed CO_2–$HOCH_2CH_2OH$ ice and 1811 cm^{-1} in irradiated $^{13}CO_2$–$HO^{13}CH_2{}^{13}CH_2OH$ ice (figs. S1 and S4) can be assigned to the *trans*-hydroxycarbonyl radical (HOĊO, ν_2) and/or formyl radical (HĊO, ν_3). Because of the matrix effect, the absorptions of fundamental (CO stretch) of *trans*-hydroxycarbonyl radical (ν_2) and formyl radical (ν_3) are close to one another (*31*, *32*) and cannot be clearly distinguished here. Because of the overlapping absorption features resulting from a wide variety of complex organic molecules produced during radiation processing, infrared spectra cannot uniquely identify complex organic molecules such as **1**, but only their functional groups, highlighting the need for an alternative analytical technique to detect individual reaction products (*33*, *34*).

Photoionization reflectron time-of-flight mass spectrometry

PI-ReTOF-MS represents an ideal technique to identify individual $C_3H_6O_4$ isomers in the gas phase based on their distinct adiabatic IEs and mass-to-charge ratios (m/z) (*33*, *35*). Separate experiments exploiting two photon energies of 11.10 and 8.77 eV were selected to distinguish the first-generation products **1** and 2-hydroxyethyl hydrogen carbonate ($HOCH_2CH_2OCOOH$, **18**) formed through radical-radical reactions as well as the second-generation product propene-1,1,2,3-tetrol [$HOCH_2CH(OH)C(OH)_2$, **19**] accessed via tautomerization of **1** (Fig. 2). Photons (11.10 eV) aid in the photoionization of all three isomers if formed, while 8.77 eV photons only ionize **19** (IE = 7.24 to 7.53 eV), but neither **1** (IE = 9.69 to 10.17 eV) nor **18** (IE = 9.79 to 11.09 eV). Figure 3 compiles the PI-ReTOF-MS of the subliming molecules from the exposed carbon dioxide–ethylene glycol ices during the TPD phase. Tentative assignments of $C_2H_4O_3$ and $C_3H_6O_3$ isomers are presented in the Supplementary Materials (figs. S7 and S8). Concentrating on the $C_3H_6O_4$ isomers, the TPD profile of the ion signal at m/z = 106 for the irradiated CO_2–$HOCH_2CH_2OH$ ice at 11.10 eV (black line, Fig. 4A) shows sublimation events at 240 K (peak 1) and 273 K (peak 2). Since the signal at m/z = 106 can be associated with the molecular formulae $C_2H_2O_5$, $C_3H_6O_4$, $C_4H_{10}O_3$, $C_6H_2O_2$, C_7H_6O, and C_8H_{10}, isotopically labeled reactants were exploited to assign the molecular formula(e). The replacement of the CO_2–$HOCH_2CH_2OH$ ice by $^{13}CO_2$–$HO^{13}CH_2{}^{13}CH_2OH$ ice shifts the m/z by 3 atomic mass unit (amu) from m/z = 106 ($C_3H_6O_4^+$) to m/z = 109 ($^{13}C_3H_6O_4^+$); this finding confirms the presence of three carbon atoms (Fig. 4A). The substitution of CO_2 by $C^{18}O_2$ results in products with two ^{18}O atoms that can be observed at m/z = 110 ($C_3H_6O_2{}^{18}O_2^+$) in the $C^{18}O_2$–$HOCH_2CH_2OH$ ice. Last, deuterated methylene (CD_2) moieties (CO_2–$HOCD_2CD_2OH$ ice) result in products with five deuterium atoms; the observed signals shift to m/z = 111 ($C_3HD_5O_4^+$) (Fig. 4B). Hence, the sublimation events (peaks 1 and 2) at m/z = 106 can be clearly assigned to a molecule of the formula $C_3H_6O_4$.

The TPD profile of m/z = 106 ($C_3H_6O_4^+$) at 11.10 eV reveals sublimation events at 240 K (peak 1) and 273 K (peak 2) (Fig. 4A). A blank experiment conducted without exposing the ices to ionizing radiation under otherwise identical conditions does not reveal any

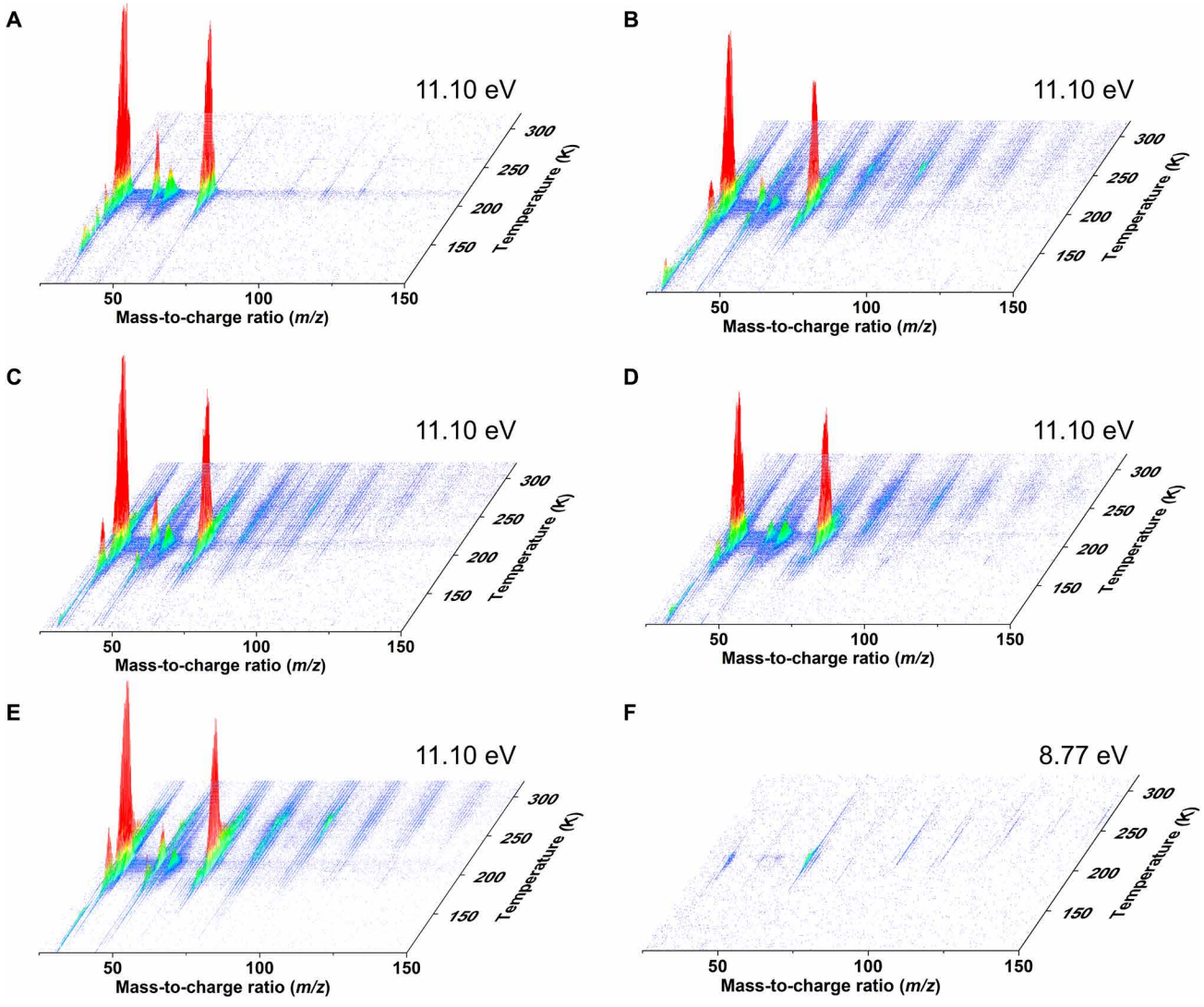

Fig. 3. PI-ReTOF-MS data as a function of temperature and *m/z* ratios during the TPD of the carbon dioxide–ethylene glycol ices. Data were recorded for the unirradiated (blank) CO_2–$HOCH_2CH_2OH$ ice at 11.10 eV (**A**), the irradiated (30 nA, 60 min) CO_2–$HOCH_2CH_2OH$ ice at 11.10 eV (**B**) and 8.77 eV (**F**), the irradiated $C^{18}O_2$–$HOCH_2CH_2OH$ ice at 11.10 eV (**C**), the irradiated CO_2–$HOCD_2CD_2OH$ ice at 11.10 eV (**D**), and the irradiated $^{13}CO_2$–$HO^{13}CH_2{}^{13}CH_2OH$ ice at 11.10 eV (**E**).

ion signal at $m/z = 106$ between 210 and 300 K (Fig. 4A). This finding confirms that peaks 1 and 2 are the results of the irradiation of the ices. At 11.10 eV, all three isomers **1** (IE = 9.69 to 10.17 eV), **18** (IE = 9.79 to 11.09 eV), and **19** (IE = 7.24 to 7.53 eV) can be ionized (Fig. 2 and table S5). Thereafter, the photon energy was reduced to 8.77 eV; at this energy, only the enol tautomer **19** can be ionized if present. However, upon reducing the photon energy to 8.77 eV, peaks 1 and 2 are absent (Fig. 4C). An additional experiment was performed with a higher dose of irradiation (100 nA, 120 min) to probe the formation of **19**. Even at this increased dose, which corresponds to 12 ± 2 eV molecule^{-1} of carbon dioxide and 21 ± 3 eV molecule^{-1} of **16**, no ion signal was detectable at $m/z = 106$, confirming the absence of **19**. Therefore, peaks 1 and 2 can only be associated with isomers **1** and/or **18**. Because of the overlap of their IEs, it is imperative to confirm their formation using isotopically labeled ices. Here, the identification of isomers **1** and **18** was achieved by exploiting partially deuterated reactants (CO_2–$HOCD_2CD_2OH$ ice) during photoionizing at 11.10 eV. This strategy is highlighted in fig. S5 and reveals that their ion signals can be separated through the detection of $m/z = 109$ [$HOCD_2CD(OH)COOH^+$] for **1** and $m/z = 111$ ($HOCD_2CD_2OCOOD^+$) for **18**. In the processed CO_2–$HOCD_2CD_2OH$ ice (Fig. 4B), the TPD profile at $m/z = 109$ only shows one sublimation event (peak 2), indicating that peak 2 is linked to **1**. For ion signals of $m/z = 111$, the TPD profile shows both peak 1 and peak 2. This is counterintuitive since only one peak connected to $m/z = 111$ ($HOCD_2CD_2OCOOD^+$) for **18** should be present. In the processed CO_2–$HOCD_2CD_2OH$ ice, it is likely that 2-hydroxyethoxy-d_4 ($\dot{O}CD_2CD_2OH$, **20**) can isomerize to **17**-d_4 ($DOC\dot{D}CD_2OH$), which then reacts with hydroxycarbonyl-d_1($DO\dot{C}O$, **11**) radical to form **1**-d_5 [$HOCD_2CD(OD)COOD^+$; $m/z = 111$], leading to the presence of peak 2. Therefore, only peak 1 can be clearly associated with **18**. This isomerization was also tackled computationally. Using the AE-CCSD(T)/CBS//AE-MP2/aug-cc-pVTZ level of theory, Wang and Bowie (*36*) calculated the

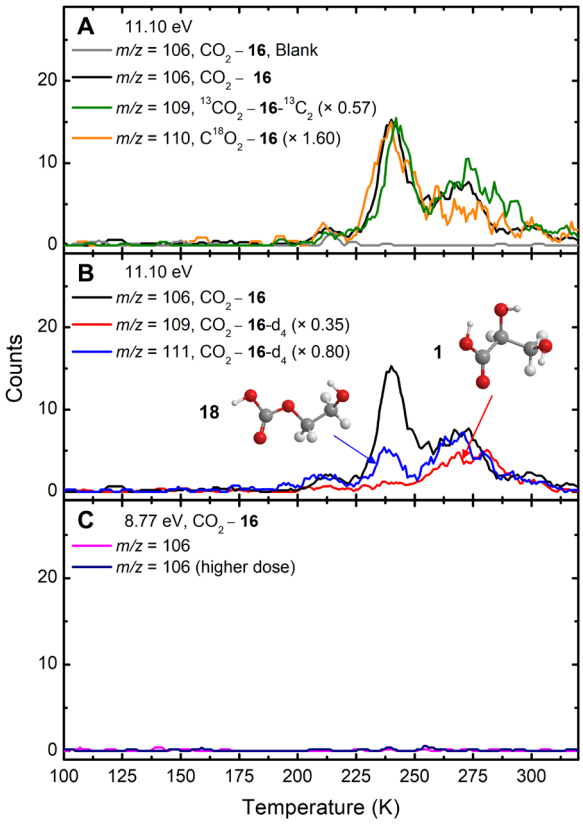

Fig. 4. Ion signal during TPD of irradiated carbon dioxide–ethylene glycol (16) ices shown as a function of temperature. (**A**) TPD profiles measured at 11.10 eV with irradiated (30 nA, 60 min) CO_2–$HOCH_2CH_2OH$ ice (m/z = 106), $^{13}CO_2$–$HO^{13}CH_2{}^{13}CH_2OH$ ice (m/z = 109), and $C^{18}O_2$–$HOCH_2CH_2OH$ ice (m/z = 110). (**B**) TPD profiles measured at 11.10 eV at m/z = 109 and m/z = 111 in irradiated (30 nA, 60 min) CO_2–$HOCD_2CD_2OH$ ice. (**C**) TPD profiles measured at 8.77 eV at m/z = 106 in CO_2–$HOCH_2CH_2OH$ ice irradiated with a low dose (30 nA, 60 min) and a higher dose (100 nA, 120 min).

isomerization reaction from 2-hydroxyethoxy ($\dot{O}CH_2CH_2OH$, **20**) radical to 1,2-dihydroxyethyl ($HO\dot{C}HCH_2OH$, **17**) radical to be exoergic (44 kJ mol^{-1}) with a reaction barrier of 117 kJ mol^{-1}; this barrier can be overcome by the kinetic energy of the incident electrons. Moreover, the sublimation sequences of **18** at 240 K and **1** at 273 K correlate with an enhanced polarity and increased number of hydroxyl groups (–OH) of the subliming isomers (*24*, *37*–*39*). In particular, **1** carries an extra hydroxyl group in comparison to **18**, leading to an increase of the sublimation temperature by 33 K. The detected counts of **1** and **18** in the CO_2–$HOCH_2CH_2OH$ system were 230 ± 20 and 270 ± 15 counts, respectively. In addition, the TPD profile of the ion signal at m/z = 106 for the irradiated CO_2–$HOCH_2CH_2OH$ ice matches the TPD profile at m/z = 89 (fig. S6), which may be caused by the photodissociation of **1** and **18** by losing a hydroxyl group (–OH) upon ionization at 11.10 eV.

Having provided compelling evidence on the preparation and detection of **1** and **18**, we shift our attention now to their formation mechanisms. First, reactions (1) to (3) lead to unimolecular decomposition of **16** to **17** [$HO\dot{C}HCH_2OH$; reaction (1)] and to **20** [$\dot{O}CH_2CH_2OH$; reaction (2)]; the suprathermal hydrogen atoms generated add to the C=O bond in carbon monoxide forming the hydroxycarbonyl radical **11**($HO\dot{C}O$) [reaction (3)]. The decomposition of **16** is endoergic by 398 ± 4 kJ mol^{-1} for reaction (1) and 443 ± 4 kJ mol^{-1} for reaction (2) (*40*, *41*); this endoergicity can be compensated for by an energy transfer from the impinging electrons to **16** (*42*). Reactions (1) and (2) closely resemble the decomposition of methanol (**10**) that produces hydroxymethyl ($\dot{C}H_2OH$) and methoxy ($CH_3\dot{O}$) radicals (*24*, *43*). Previous work by Song *et al.* (*3*) revealed that reaction is exoergic by 22 kJ mol^{-1} with an entrance barrier of 106 kJ mol^{-1} (1.1 eV) calculated at the MRCISD+Q/cc-pVTZ//CASSCF/cc-pVTZ level of theory (*44*). Note that gas-phase calculations may overestimate the real barrier of the reactions because nearby molecules in the ice phase could be involved in the reaction mechanism (*45*, *46*). Furthermore, the suprathermal hydrogen atoms have excess kinetic energy of a few electron volts (*47*); this energy can be used to overcome the entrance barrier of reaction (3), leading eventually to **11** (*35*) as identified through FTIR spectroscopy at 1849 cm^{-1} for **11** (ν_2; $HO\dot{C}O$) in irradiated CO_2–$HOCH_2CH_2OH$ ice and at 1811 cm^{-1} for **11**-^{13}C (ν_2; $HO^{13}\dot{C}O$) in irradiated $^{13}CO_2$–$HO^{13}CH_2{}^{13}CH_2OH$ ice.

$$HOCH_2CH_2OH\,(\mathbf{16}) \rightarrow HO\dot{C}HCH_2OH\,(\mathbf{17}) + \dot{H} \quad (1)$$

$$HOCH_2CH_2OH\,(\mathbf{16}) \rightarrow \dot{O}CH_2CH_2OH\,(\mathbf{20}) + \dot{H} \quad (2)$$

$$CO_2 + \dot{H} \rightarrow HO\dot{C}O\ (\mathbf{11}) \quad (3)$$

Second, the preparation of **1** and **18** relies on barrierless radical-radical recombination of **11** with **17** [reaction (4)] and **20** [reaction (5)] radicals, respectively. Recall that the TPD profile at m/z = 106 ($C_3H_6O_4^+$) in CO_2–$HOCH_2CH_2OH$ ice shifts 4 amu to m/z = 110 ($C_3H_6O_2{}^{18}O_2^+$) in $C^{18}O_2$–$HOCH_2CH_2OH$ ice and 5 amu to m/z = 111 ($C_3HD_5O_4^+$) in CO_2–$HOCD_2CD_2OH$ ice (Fig. 4), indicating that the formation of **1** or **18** involves one carbon dioxide and one **16** molecule.

$$HO\dot{C}O\,(\mathbf{11}) + HO\dot{C}HCH_2OH\,(\mathbf{17}) \rightarrow HOCH_2CH(OH)COOH\,(\mathbf{1}) \quad (4)$$

$$HO\dot{C}O\,(\mathbf{11}) + \dot{O}CH_2CH_2OH\,(\mathbf{20}) \rightarrow HOCH_2CH_2OCOOH\,(\mathbf{18}) \quad (5)$$

DISCUSSION

In conclusion, this study presents an abiotic route to a key biomolecule glyceric acid (**1**)—the simplest sugar acid—via barrierless radical-radical recombination of **11** with **17**, providing crucial steps toward a systematic understanding of how sugar acids can be formed in carbon dioxide–containing interstellar ices. **1** and its isomer 2-hydroxyethyl hydrogen carbonate (**18**) were formed in interstellar model ices of carbon dioxide and ethylene glycol upon exposure to ionizing radiation at low temperatures of 5 K. Using tunable PI-ReTOF-MS along with isotopic labeling experiments, **1** and **18** were detected in the gas phase during the TPD. The overall reaction energy leading to **1** from carbon dioxide and **16** [reactions (1), (3), and (4)] is endoergic by 35 kJ mol^{-1} as compensated by the kinetic energy of the incident electrons (*41*, *48*), thus highlighting the necessity of nonequilibrium chemistry in its formation in the ISM. Carbon dioxide and **16** are abundant in the ISM and have both been detected in molecular clouds such as Orion-KL—the star-forming region of the Orion Nebula (*25*, *49*), and the presence of **1** and **18** in interstellar environments is therefore plausible. Thus, the hitherto

astronomically unobserved **1** and **18** represent promising candidates for future astronomical searches via gas-phase rotational emissions exploiting telescopes such as the Atacama Large Millimeter/submillimeter Array (ALMA). Once formed within interstellar ices in cold molecular clouds, **1** and **18** can be incorporated into accreting planetoids, asteroids, and comets (*50*). Ultimately, a fraction of these molecules can be delivered to planets like the early Earth and act as an exogenous source of biomolecules and their feedstocks (*6*). Detailed analyses of meteorites such as Murchison revealed that not only sugar-related organic compounds including **1** but also amino acids and dipeptides can be embedded in meteoritic matter and survive the harsh conditions in space and impact on the Earth (*1*, *51*, *52*). Therefore, a firm detection of **1** in the ISM in conjunction with rigorous modeling studies of reaction pathways to form prebiotic biorelevant molecules (Fig. 1) in deep space is of particular importance to our understanding of the role of sugar acids for the molecular complexity and synthesis of key organic molecules linked to the origin of life (*35*, *53*, *54*).

MATERIALS AND METHODS

Experimental

Experiments were carried out in a hydrocarbon-free stainless steel chamber under ultrahigh vacuum conditions maintained at pressures of a few 10^{-11} torr by magnetically levitated turbomolecular pumps (Osaka, TG1300MUCWB and TG420MCAB), which are backed by a dry scroll pump (XDS35i, BOC Edwards) (*55*). A polished silver substrate (12.6 mm × 15.1 mm) for ice deposition was attached to a two-stage closed-cycle helium refrigerator (Sumitomo Heavy Industries, RDK-415E) that can be freely rotated and translated vertically. The chemical samples used in the experiment were carbon dioxide–$^{18}O_2$ ($C^{18}O_2$, Sigma-Aldrich, 95 atom % ^{18}O), carbon dioxide–^{13}C ($^{13}CO_2$, Sigma-Aldrich, 99 atom % ^{13}C), carbon dioxide (CO_2, Airgas, 99.999%), deuterated ethylene glycol-d_4 ($HOCD_2CD_2OH$, CDN isotopes, 98.9 atom % D), ethylene glycol–$^{13}C_2$ ($HO^{13}CH_2{}^{13}CH_2OH$, Sigma-Aldrich, 99 atom % ^{13}C), and ethylene glycol ($HOCH_2CH_2OH$, Sigma-Aldrich, anhydrous, 99.8%). Ethylene glycol sample was stored in a borosilicate vial that was connected to a high vacuum chamber at pressures of a few 10^{-8} torr and subjected to several freeze-pump-thaw cycles to remove residual atmospheric gases. Ices were prepared by passing carbon dioxide gas and ethylene glycol vapor through separate glass capillary arrays directed at the wafer cooled to 5.0 ± 0.3 K. Partial pressures were 2×10^{-8} torr for carbon dioxide and 4×10^{-9} torr for ethylene glycol. Ice thickness was measured during the deposition via laser interferometry (*56*); a photodiode was used to record variations in the intensity of a helium-neon laser (CVI Melles Griot, 25-LHP-230; 632.8 nm) reflected from the ice and silver substrate resulting from thin-film interference. The concentration-weighted average index of 1.32 ± 0.09 was used to derive the thickness of the carbon dioxide–ethylene glycol ices from the refractive indexes of amorphous carbon dioxide ice (n = 1.21) at 10 K (*57*) and that of ethylene glycol ice (n = 1.43) (*58*). Ice thicknesses were determined to be 750 ± 80 nm (table S6) by taking into account the densities of carbon dioxide (0.98 g cm^{-3}) (*57*) and ethylene glycol (1.1 g cm^{-3}) (*59*). To monitor the changes of ices in situ before and after the deposition, an FTIR spectrometer (Thermo Electron, Nicolet 6700) was used in the range of 6000 to 500 cm^{-1} with 4 cm^{-1} spectral resolution. The ratio of carbon dioxide to ethylene glycol in the ice was determined to be 2.1 ± 0.7:1 using the integrated infrared absorptions of carbon dioxide at 3701 cm^{-1} ($\nu_1 + \nu_3$, 1.8×10^{-18} cm $molecule^{-1}$) and 2278 cm^{-1} [ν_3 ($^{13}CO_2$), 6.8×10^{-17} cm $molecule^{-1}$] (*27*) and the absorption bands of pure ethylene glycol ice with known thickness (fig. S9).

After the deposition, the ice mixtures were irradiated with 5-keV electrons (SPECS, EQ PU-22) at a 70° angle of incidence for 60 min at a current of 30 nA. On the basis of Monte Carlo simulations performed with the CASINO software suite (*60*), the irradiation conditions correspond to doses of 1.8 ± 0.3 eV $molecule^{-1}$ for carbon dioxide and 3.1 ± 0.5 eV $molecule^{-1}$ for ethylene glycol, respectively, simulating secondary electrons generated in the track of GCRs in cold molecular clouds aged around 5×10^6 years (*22*). The average penetration depth of electrons in CO_2–$HOCH_2CH_2OH$ ice was calculated to be 300 ± 60 nm based on Monte Carlo simulations using CASINO 2.42 (*60*). The penetration depth is notably less than the ice thickness (750 ± 80 nm), preventing electron-initiated interactions between the ice and the silver substrate. The changes in the spectrum of the ices were monitored by the FTIR spectrometer before, during, and after irradiation. After irradiation, the ices were subjected to TPD and heated from 5 to 320 K at 0.5 K min^{-1}. Subliming molecules were photoionized 2 mm above the ice surface by pulsed 30-Hz VUV light at 11.10 or 8.77 eV, which was generated through resonant four-wave mixing ($\omega_{VUV} = 2\omega_1 \pm \omega_2$) schemes using Xenon as a nonlinear medium (table S7). The VUV photons were generated via sum frequency generation ($2\omega_1 + \omega_2$; 11.10 eV) and difference frequency generation ($2\omega_1 - \omega_2$; 8.77 eV) with 249.628 nm (ω_1; dye laser, Sirah Lasertechnik, Cobra-Stretch) and 1064 nm (ω_2; Nd:YAG laser, Spectra-Physics, Quanta Ray PRO 270-30) (*12*). A biconvex lithium fluoride lens (Korth Kristalle, R1 = R2 = 131 mm) was used in an off-axis geometry to spatially separate the VUV light from other laser beams. The ions resulting from VUV photoionization were mass-analyzed via ReTOF-MS and detected with a dual microchannel plate (MCP) detector in the chevron configuration (Jordan TOF Products). The MCP signal was amplified with a preamplifier (Ortec, 9305), discriminated (Advanced Research Instruments Corp., F100-TD), and recorded by a multichannel scaler (FAST ComTec, MCS6A, 30 Hz). For each recorded mass spectra, the accumulation time of ion signals was 2 min (3600 sweeps) and the ion arrival time was recorded to 3.2-ns accuracy. Recorded TPD profiles were corrected for variations in the VUV flux throughout each experiment, which was monitored during TPD via a Faraday cup (*61*). Additional experiment was also performed without irradiation (blank) at 11.10 eV for carbon dioxide–ethylene glycol ice, and no ion signal at m/z = 106 was observed.

Computational

The adiabatic IEs and relative energies are computed as zero-point vibrational energy (ZPVE) corrected adiabatic differences in the energies of the neutral and radical-cation geometries. B3LYP/aug-cc-pVTZ was used to optimize the geometries and compute the harmonic vibrational energies in Gaussian16 (*62*–*66*). Explicitly correlated coupled-cluster singles, doubles, and perturbative triples [CCSD(T)-F12b] using the cc-pVTZ-F12 basis set as available within MOLPRO 2020.1 program (*67*–*71*) produced single-point energies of $C_3H_6O_4$ isomers at the optimized B3LYP/aug-cc-pVTZ geometries. These CCSD(T)-F12b energies along with the B3LYP ZPVEs produce the IEs and relative energies (table S5). The CCSD(T)-F12b/cc-pVTZ-F12 single-point energy of PBE0/aug-cc-pVTZ and ωB97XD/aug-cc-pVTZ anharmonic vibrational analysis for both density functionals were calculated for **1** and **18**; the shifts in IE and relative energy are shown in table S8. This approach has demonstrated a good correlation with experiments in previous work (*72*). The computed Cartesian

coordinates and harmonic and anharmonic vibrational frequencies are listed in table S9.

Supplementary Materials

This PDF file includes:

Tentative assignments of $C_2H_4O_3$ and $C_3H_6O_3$ isomers
Figs. S1 to S9
Tables S1 to S9
References

REFERENCES AND NOTES

1. G. Cooper, N. Kimmich, W. Belisle, J. Sarinana, K. Brabham, L. Garrel, Carbonaceous meteorites as a source of sugar-related organic compounds for the early Earth. *Nature* **414**, 879–883 (2001).
2. G. Cooper, A. C. Rios, Enantiomer excesses of rare and common sugar derivatives in carbonaceous meteorites. *Proc. Natl. Acad. Sci. U.S.A.* **113**, E3322–E3331 (2016).
3. G. Cooper, A. C. Rios, M. Nuevo, Monosaccharides and their derivatives in carbonaceous meteorites: A scenario for their synthesis and onset of enantiomeric excesses. *Life* **8**, 36 (2018).
4. C. Zhu, A. M. Turner, C. Meinert, R. I. Kaiser, On the production of polyols and hydroxycarboxylic acids in interstellar analogous ices of methanol. *Astrophys. J.* **889**, 134 (2020).
5. S. A. Sandford, M. Nuevo, P. P. Bera, T. J. Lee, Prebiotic astrochemistry and the formation of molecules of astrobiological interest in interstellar clouds and protostellar disks. *Chem. Rev.* **120**, 4616–4659 (2020).
6. R. F. Martínez, L. A. Cuccia, C. Viedma, P. Cintas, On the origin of sugar handedness: Facts, hypotheses and missing links—A review. *Orig. Life Evol. Biosph.* **52**, 21–56 (2022).
7. J. Bocková, N. C. Jones, V. Leyva, M. Gaysinski, S. V. Hoffmann, C. Meinert, Concentration and pH effect on the electronic circular dichroism and anisotropy spectra of aqueous solutions of glyceric acid calcium salt. *Chirality* **34**, 245–252 (2022).
8. V. Kolb, L. E. Orgel, Phosphorylation of glyceric acid in aqueous solution using trimetaphosphate. *Orig. Life Evol. Biosph.* **26**, 7–13 (1996).
9. M. Scheffen, D. G. Marchal, T. Beneyton, S. K. Schuller, M. Klose, C. Diehl, J. Lehmann, P. Pfister, M. Carrillo, H. He, S. Aslan, N. S. Cortina, P. Claus, D. Bollschweiler, J.-C. Baret, J. M. Schuller, J. Zarzycki, A. Bar-Even, T. J. Erb, A new-to-nature carboxylation module to improve natural and synthetic CO_2 fixation. *Nat. Catal.* **4**, 105–115 (2021).
10. J. Velíšek, K. Cejpek, Biosynthesis of food constituents: Lipids. 2. Triacylglycerols, glycerophospholipids, and glyceroglycolipids—A review. *Czech J. Food Sci.* **24**, 241–254 (2006).
11. K. Ruiz-Mirazo, C. Briones, A. de la Escosura, Prebiotic systems chemistry: New perspectives for the origins of life. *Chem. Rev.* **114**, 285–366 (2014).
12. J. H. Marks, J. Wang, M. M. Evseev, O. V. Kuznetsov, I. O. Antonov, R. I. Kaiser, Complex reactive acids from methanol and carbon dioxide ice: Glycolic acid ($HOCH_2COOH$) and carbonic acid monomethyl ester (CH_3OCOOH). *Astrophys. J.* **942**, 43 (2023).
13. C.-H. Zhou, J. N. Beltramini, Y.-X. Fan, G. Q. Lu, Chemoselective catalytic conversion of glycerol as a biorenewable source to valuable commodity chemicals. *Chem. Soc. Rev.* **37**, 527–549 (2008).
14. C. H. Zhou, H. Zhao, D. S. Tong, L. M. Wu, W. H. Yu, Recent advances in catalytic conversion of glycerol. *Catal. Rev. Sci. Eng.* **55**, 369–453 (2013).
15. R. I. Kaiser, S. Maity, B. M. Jones, Synthesis of prebiotic glycerol in interstellar ices. *Angew. Chem. Int. Ed.* **54**, 195–200 (2015).
16. B. A. McGuire, Census of interstellar, circumstellar, extragalactic, protoplanetary disk, and exoplanetary molecules. *Astrophys. J. Suppl. Ser.* **259**, 30 (2022).
17. J. M. Hollis, F. J. Lovas, P. R. Jewell, Interstellar glycolaldehyde: The first sugar. *Astrophys. J.* **540**, L107–L110 (2000).
18. J. M. Hollis, F. J. Lovas, P. R. Jewell, L. H. Coudert, Interstellar antifreeze: Ethylene glycol. *Astrophys. J.* **571**, L59–L62 (2002).
19. M. Nuevo, J. H. Bredehöft, U. J. Meierhenrich, L. d'Hendecourt, W. H.-P. Thiemann, Urea, glycolic acid, and glycerol in an organic residue produced by ultraviolet irradiation of interstellar/pre-cometary ice analogs. *Astrobiology* **10**, 245–256 (2010).
20. C. Meinert, I. Myrgorodska, P. de Marcellus, T. Buhse, L. Nahon, S. V. Hoffmann, L. L. S. d'Hendecourt, U. J. Meierhenrich, Ribose and related sugars from ultraviolet irradiation of interstellar ice analogs. *Science* **352**, 208–212 (2016).
21. C. Chyba, C. Sagan, Endogenous production, exogenous delivery and impact-shock synthesis of organic molecules: An inventory for the origins of life. *Nature* **355**, 125–132 (1992).
22. A. G. Yeghikyan, Irradiation of dust in molecular clouds. II. Doses produced by cosmic rays. *Astrophysics* **54**, 87–99 (2011).
23. E. L. Gibb, D. C. B. Whittet, A. C. A. Boogert, A. G. G. M. Tielens, Interstellar ice: The infrared space observatory legacy. *Astrophys. J. Suppl. Ser.* **151**, 35–73 (2004).
24. C. Zhu, R. Frigge, A. Bergantini, R. C. Fortenberry, R. I. Kaiser, Untangling the formation of methoxymethanol (CH_3OCH_2OH) and dimethyl peroxide (CH_3OOCH_3) in star-forming regions. *Astrophys. J.* **881**, 156 (2019).
25. N. Brouillet, D. Despois, X.-H. Lu, A. Baudry, J. Cernicharo, D. Bockelée-Morvan, J. Crovisier, N. Biver, Antifreeze in the hot core of Orion—First detection of ethylene glycol in Orion-KL. *Astron. Astrophys.* **576**, A129 (2015).
26. J. Crovisier, D. Bockelée-Morvan, N. Biver, P. Colom, D. Despois, D. C. Lis, Ethylene glycol in comet C/1995 O1 (Hale-Bopp). *Astron. Astrophys.* **418**, L35–L38 (2004).
27. M. Bouilloud, N. Fray, Y. Benilan, H. Cottin, M. C. Gazeau, A. Jolly, Bibliographic review and new measurements of the infrared band strengths of pure molecules at 25 K: H_2O, CO_2, CO, CH_4, NH_3, CH_3OH, HCOOH and H_2CO. *Mon. Notices Royal Astron. Soc.* **451**, 2145–2160 (2015).
28. M. E. Jacox, The spectroscopy of molecular reaction intermediates trapped in the solid rare gases. *Chem. Soc. Rev.* **31**, 108–115 (2002).
29. T. Butscher, F. Duvernay, G. Danger, T. Chiavassa, Radical-induced chemistry from VUV photolysis of interstellar ice analogues containing formaldehyde. *Astron. Astrophys.* **593**, A60 (2016).
30. M. M. Wohar, P. W. Jagodzinski, Infrared spectra of H_2CO, $H_2{}^{13}CO$, D_2CO, and $D_2{}^{13}CO$ and anomalous values in vibrational force fields. *J. Mol. Spectrosc.* **148**, 13–19 (1991).
31. D. E. Milligan, M. E. Jacox, Infrared spectrum and structure of intermediates in the reaction of OH with CO. *J. Chem. Phys.* **54**, 927–942 (1971).
32. D. E. Milligan, M. E. Jacox, Infrared spectrum of HCO. *J. Chem. Phys.* **41**, 3032–3036 (1964).
33. A. M. Turner, R. I. Kaiser, Exploiting photoionization reflectron time-of-flight mass spectrometry to explore molecular mass growth processes to complex organic molecules in interstellar and solar system ice analogs. *Acc. Chem. Res.* **53**, 2791–2805 (2020).
34. J. Wang, J. H. Marks, A. M. Turner, A. A. Nikolayev, V. Azyazov, A. M. Mebel, R. I. Kaiser, Mechanistical study on the formation of hydroxyacetone (CH_3COCH_2OH), methyl acetate (CH_3COOCH_3), and 3-hydroxypropanal ($HCOCH_2CH_2OH$) along with their enol tautomers (prop-1-ene-1,2-diol ($CH_3C(OH)CHOH$), prop-2-ene-1,2-diol ($CH_2C(OH)CH_2OH$), 1-methoxyethen-1-ol ($CH_3OC(OH)CH_2$) and prop-1-ene-1,3-diol ($HOCH_2CHCHOH$)) in interstellar ice analogs. *Phys. Chem. Chem. Phys.* **25**, 936–953 (2023).
35. N. F. Kleimeier, A. K. Eckhardt, P. R. Schreiner, R. I. Kaiser, Interstellar formation of biorelevant pyruvic acid ($CH_3COCOOH$). *Chem* **6**, 3385–3395 (2020).
36. T. Wang, J. H. Bowie, Hydrogen tunnelling influences the isomerisation of some small radicals of interstellar importance. A theoretical investigation. *Org. Biomol. Chem.* **10**, 3219–3228 (2012).
37. R. I. Kaiser, S. Maity, B. M. Jones, Infrared and reflectron time-of-flight mass spectroscopic analysis of methane (CH_4)–carbon monoxide (CO) ices exposed to ionization radiation—Toward the formation of carbonyl-bearing molecules in extraterrestrial ices. *Phys. Chem. Chem. Phys.* **16**, 3399–3424 (2014).
38. A. Bergantini, R. Frigge, R. I. Kaiser, Constraining the molecular complexity in the interstellar medium—The formation of ethyl methyl ether ($CH_3OCH_2CH_3$) in star-forming regions. *Astrophys. J.* **859**, 59 (2018).
39. C. Zhu, N. F. Kleimeier, A. M. Turner, S. K. Singh, R. C. Fortenberry, R. I. Kaiser, Synthesis of methanediol [$CH_2(OH)_2$]: The simplest geminal diol. *Proc. Natl. Acad. Sci. U.S.A.* **119**, e2111938119 (2022).
40. C. F. Goldsmith, G. R. Magoon, W. H. Green, Database of small molecule thermochemistry for combustion. *J. Phys. Chem. A* **116**, 9033–9057 (2012).
41. B. Ruscic, H. Bross, Active Thermochemical Tables (ATcT) values based on ver. 1.122r of the Thermochemical Network (ATcT.anl.gov, 2021).
42. R. I. Kaiser, G. Eich, A. Gabrysch, K. Roessler, Theoretical and laboratory studies on the interaction of cosmic-ray particles with interstellar ices. II. Formation of atomic and molecular hydrogen in frozen organic molecules. *Astrophys. J.* **484**, 487–498 (1997).
43. C. J. Bennett, S. H. Chen, B. J. Sun, A. H. H. Chang, R. I. Kaiser, Mechanistical studies on the irradiation of methanol in extraterrestrial ices. *Astrophys. J.* **660**, 1588–1608 (2007).
44. X. Song, J. Li, H. Hou, B. Wang, Ab initio study of the potential energy surface for the $OH+CO \rightarrow H+CO_2$ reaction. *J. Chem. Phys.* **125**, 094301 (2006).
45. J. Wang, A. A. Nikolayev, J. H. Marks, M. McAnally, V. N. Azyazov, A. K. Eckhardt, A. M. Mebel, R. I. Kaiser, Quantum tunneling mediated low-temperature synthesis of interstellar hemiacetals. *J. Phys. Chem. Lett.* **14**, 6078–6085 (2023).
46. J. H. Marks, A. A. Nikolayev, M. M. Evseev, J. Wang, A. M. Turner, N. F. Kleimeier, O. V. Kuznetsov, M. McAnally, A. N. Morozov, I. O. Antonov, A. M. Mebel, R. I. Kaiser, Quantum-tunneling-mediated synthesis of prebiotic chelation agents in interstellar analog ices. *Chem* **9**, 3286–3303 (2023).
47. C. Zhu, A. Bergantini, S. K. Singh, M. J. Abplanalp, R. I. Kaiser, Rapid radical–radical induced explosive desorption of ice-coated interstellar nanoparticles. *Astrophys. J.* **920**, 73 (2021).
48. M. Vasiliu, A. J. Jones, K. Guynn, D. A. Dixon, Prediction of the thermodynamic properties of key products and intermediates from Biomass. II. *J. Phys. Chem. C* **116**, 20738–20754 (2012).
49. A. M. S. Boonman, E. F. van Dishoeck, F. Lahuis, S. D. Doty, C. M. Wright, D. Rosenthal, Gas-phase CO_2, C_2H_2, and HCN toward Orion-KL. *Astron. Astrophys.* **399**, 1047–1061 (2003).

50. Y. Furukawa, Y. Chikaraishi, N. Ohkouchi, N. O. Ogawa, D. P. Glavin, J. P. Dworkin, C. Abe, T. Nakamura, Extraterrestrial ribose and other sugars in primitive meteorites. *Proc. Natl. Acad. Sci. U.S.A.* **116**, 24440–24445 (2019).
51. J. R. Cronin, C. B. Moore, Amino acid analyses of the Murchison, Murray, and Allende carbonaceous chondrites. *Science* **172**, 1327–1329 (1971).
52. A. Shimoyama, R. Ogasawara, Dipeptides and diketopiperazines in the Yamato-791198 and Murchison carbonaceous chondrites. *Orig. Life Evol. Biosph.* **32**, 165–179 (2002).
53. A. L. Weber, Thermal synthesis and hydrolysis of polyglyceric acid. *Orig. Life Evol. Biosph.* **19**, 7–19 (1989).
54. D. P. Glavin, A. S. Burton, J. E. Elsila, J. C. Aponte, J. P. Dworkin, The search for chiral asymmetry as a potential biosignature in our solar system. *Chem. Rev.* **120**, 4660–4689 (2020).
55. B. M. Jones, R. I. Kaiser, Application of reflectron time-of-flight mass spectroscopy in the analysis of astrophysically relevant ices exposed to ionization radiation: Methane (CH_4) and D4-methane (CD_4) as a case study. *J. Phys. Chem. Lett.* **4**, 1965–1971 (2013).
56. A. M. Turner, M. J. Abplanalp, S. Y. Chen, Y. T. Chen, A. H. Chang, R. I. Kaiser, A photoionization mass spectroscopic study on the formation of phosphanes in low temperature phosphine ices. *Phys. Chem. Chem. Phys.* **17**, 27281–27291 (2015).
57. M. Á. Satorre, M. Domingo, C. Millán, R. Luna, R. Vilaplana, C. Santonja, Density of CH_4, N_2 and CO_2 ices at different temperatures of deposition. *Planet. Space Sci.* **56**, 1748–1752 (2008).
58. C. Pale-Grosdemange, E. S. Simon, K. L. Prime, G. M. Whitesides, Formation of self-assembled monolayers by chemisorption of derivatives of oligo(ethylene glycol) of structure $HS(CH_2)_{11}(OCH_2CH_2)_mOH$ on gold. *J. Am. Chem. Soc.* **113**, 12–20 (1991).
59. R. L. Hudson, M. H. Moore, A. M. Cook, IR characterization and radiation chemistry of glycolaldehyde and ethylene glycol ices. *Adv. Space Res.* **36**, 184–189 (2005).
60. D. Drouin, A. R. Couture, D. Joly, X. Tastet, V. Aimez, R. Gauvin, CASINO V2.42—A fast and easy-to-use modeling tool for scanning electron microscopy and microanalysis users. *Scanning* **29**, 92–101 (2007).
61. N. F. Kleimeier, A. K. Eckhardt, R. I. Kaiser, Identification of glycolaldehyde enol (HOHC═CHOH) in interstellar analogue ices. *J. Am. Chem. Soc.* **143**, 14009–14018 (2021).
62. W. Yang, R. G. Parr, C. Lee, Various functionals for the kinetic energy density of an atom or molecule. *Phys. Rev. A* **34**, 4586–4590 (1986).
63. A. D. Becke, Density-functional exchange-energy: Approximation with correct asymptotic behavior. *Phys. Rev. A* **38**, 3098–3100 (1988).
64. T. H. Dunning, Gaussian basis sets for use in correlated molecular calculations. I. The atoms boron through neon and hydrogen. *J. Chem. Phys.* **90**, 1007–1023 (1989).
65. A. D. Becke, Density-functional thermochemistry. III. The role of exact exchange. *J. Chem. Phys.* **98**, 5648–5652 (1993).
66. G. W. T. M. J. Frisch, H. B. Schlegel, G. E. Scuseria, M. A. Robb, J. R. Cheeseman, G. Scalmani, V. Barone, G. A. Petersson, H. Nakatsuji, X. Li, M. Caricato, A. V. Marenich, J. Bloino, B. G. Janesko, R. Gomperts, B. Mennucci, H. P. Hratchian, J. V. Ortiz, A. F. Izmaylov, J. L. Sonnenberg, D. Williams-Young, F. Ding, F. Lipparini, F. Egidi, J. Goings, B. Peng, A. Petrone, T. Henderson, D. Ranasinghe, V. G. Zakrzewski, J. Gao, N. Rega, G. Zheng, W. Liang, M. Hada, M. Ehara, K. Toyota, R. Fukuda, J. Hasegawa, M. Ishida, T. Nakajima, Y. Honda, O. Kitao, H. Nakai, T. Vreven, K. Throssell, J. A. Montgomery Jr., J. E. Peralta, F. Ogliaro, M. J. Bearpark, J. J. Heyd, E. N. Brothers, K. N. Kudin, V. N. Staroverov, T. A. Keith, R. Kobayashi, J. Normand, K. Raghavachari, A. P. Rendell, J. C. Burant, S. S. Iyengar, J. Tomasi, M. Cossi, J. M. Millam, M. Klene, C. Adamo, R. Cammi, J. W. Ochterski, R. L. Martin, K. Morokuma, O. Farkas, J. B. Foresman, D. J. Fox (Gaussian Inc., Wallingford, CT, 2016).
67. K. Raghavachari, G. W. Trucks, J. A. Pople, M. Head-Gordon, A fifth-order perturbation comparison of electron correlation theories. *Chem. Phys. Lett.* **157**, 479–483 (1989).
68. T. B. Adler, G. Knizia, H.-J. Werner, A simple and efficient CCSD(T)-F12 approximation. *J. Chem. Phys.* **127**, 221106 (2007).
69. K. A. Peterson, T. B. Adler, H.-J. Werner, Systematically convergent basis sets for explicitly correlated wavefunctions: The atoms H, He, B–Ne, and Al–Ar. *J. Chem. Phys.* **128**, 084102 (2008).
70. G. Knizia, T. B. Adler, H.-J. Werner, Simplified CCSD(T)-F12 methods: Theory and benchmarks. *J. Chem. Phys.* **130**, 054104 (2009).
71. H.-J. Werner, P. J. Knowles, F. R. Manby, J. A. Black, K. Doll, A. Heßelmann, D. Kats, A. Köhn, T. Korona, D. A. Kreplin, Q. Ma, T. F. Miller III, A. Mitrushchenkov, K. A. Peterson, I. Polyak, G. Rauhut, M. Sibaev, The Molpro quantum chemistry package. *J. Chem. Phys.* **152**, 144107 (2020).
72. C. Zhang, A. M. Turner, J. Wang, J. H. Marks, R. C. Fortenberry, R. I. Kaiser, Low-temperature thermal formation of the cyclic methylphosphonic acid trimer [*c*-$(CH_3PO_2)_3$]. *ChemPhysChem* **24**, e202200660 (2023).
73. P. Buckley, P. A. Giguère, Infrared studies on rotational isomerism. I. Ethylene glycol. *Can. J. Chem.* **45**, 397–407 (1967).
74. S. Maity, R. I. Kaiser, B. M. Jones, Formation of complex organic molecules in methanol and methanol–carbon monoxide ices exposed to ionizing radiation—A combined FTIR and reflectron time-of-flight mass spectrometry study. *Phys. Chem. Chem. Phys.* **17**, 3081–3114 (2015).
75. M. E. Jacox, The vibrational spectrum of the *t*-HOCO free radical trapped in solid argon. *J. Chem. Phys.* **88**, 4598–4607 (1988).
76. R. L. Hudson, M. J. Loeffler, Ketene formation in interstellar ices: A laboratory study. *Astrophys. J.* **773**, 109 (2013).

Acknowledgments

Funding: The Hawaii group acknowledges support from the U.S. National Science Foundation, Division of Astronomical Sciences under grant AST-2103269 awarded to the University of Hawaii at Manoa (R.I.K.). The construction of the experimental setup was financed by the W. M. Keck Foundation and the University of Hawaii at Manoa. R.C.F. acknowledges support from NASA grants NNX17AH15G and NNH22ZHA004C, startup funds provided by the University of Mississippi, and computational support from the Mississippi Center for Supercomputing Research funded in part by NSF grants CHE-1338056 and OIA-1757220.
Author contributions: R.I.K. designed the experiments and directed the overall project. J.W. and J.H.M. performed all experiments. J.W. performed the data analyses. R.C.F. carried out the theoretical analysis. J.W., R.C.F., and R.I.K. wrote the manuscript, which was read, revised, and approved by all coauthors. **Competing interests:** The authors declare that they have no competing interests. **Data and materials availability:** All data needed to evaluate the conclusions in the paper are present in the paper and/or the Supplementary Materials.

Submitted 11 October 2023
Accepted 8 February 2024
Published 13 March 2024
10.1126/sciadv.adl3236